A&A 536, A1 (2011)
DOI: 10.1051/0004-6361/201116464

Astronomy & Astrophysics
Special feature

Planck early results

Planck early results. I. The *Planck* mission⋆

Planck Collaboration: P. A. R. Ade[82], N. Aghanim[54], M. Arnaud[68], M. Ashdown[66,4], J. Aumont[54], C. Baccigalupi[80], M. Baker[37], A. Balbi[31], A. J. Banday[89,9,73], R. B. Barreiro[62], J. G. Bartlett[3,64], E. Battaner[91], K. Benabed[55], K. Bennett[38], A. Benoît[53], J.-P. Bernard[89,9], M. Bersanelli[28,46], R. Bhatia[5], J. J. Bock[64,10], A. Bonaldi[42], J. R. Bond[6], J. Borrill[72,84], F. R. Bouchet[55], T. Bradshaw[79], M. Bremer[38], M. Bucher[3], C. Burigana[45], R. C. Butler[45], P. Cabella[31], C. M. Cantalupo[72], B. Cappellini[46], J.-F. Cardoso[69,3,55], R. Carr[35], M. Casale[35], A. Catalano[3,67], L. Cayón[21], A. Challinor[59,66,12], A. Chamballu[51], J. Charra[54], R.-R. Chary[52], L.-Y. Chiang[58], C. Chiang[20], P. R. Christensen[76,32], D. L. Clements[51], S. Colombi[55], F. Couchot[71], A. Coulais[67], B. P. Crill[64,77], G. Crone[38], M. Crook[79], F. Cuttaia[45], L. Danese[80], O. D'Arcangelo[63], R. D. Davies[65], R. J. Davis[65], P. de Bernardis[27], J. de Bruin[37], G. de Gasperis[31], A. de Rosa[45], G. de Zotti[42,80], J. Delabrouille[3], J.-M. Delouis[55], F.-X. Désert[49], J. Dick[80], C. Dickinson[65], K. Dolag[73], H. Dole[54], S. Donzelli[46,60], O. Doré[64,10], U. Dörl[73], M. Douspis[54], X. Dupac[36], G. Efstathiou[59], T. A. Enßlin[73], H. K. Eriksen[60], F. Finelli[45], S. Foley[37], O. Forni[89,9], P. Fosalba[56], M. Frailis[44], E. Franceschi[45], M. Freschi[36], T. C. Gaier[64], S. Galeotta[44], J. Gallegos[36], B. Gandolfo[37], K. Ganga[3,52], M. Giard[89,9], G. Giardino[38], G. Gienger[37], Y. Giraud-Héraud[3], J. González[35], J. González-Nuevo[80], K. M. Górski[64,93], S. Gratton[66,59], A. Gregorio[29], A. Gruppuso[45], G. Guyot[48], J. Haissinski[71], F. K. Hansen[60], D. Harrison[59,66], G. Helou[10], S. Henrot-Versillé[71], C. Hernández-Monteagudo[73], D. Herranz[62], S. R. Hildebrandt[10,70,61], E. Hivon[55], M. Hobson[4], W. A. Holmes[64], A. Hornstrup[14], W. Hovest[73], R. J. Hoyland[61], K. M. Huffenberger[92], A. H. Jaffe[51], T. Jagemann[36], W. C. Jones[20], J. J. Juillet[87], M. Juvela[19], P. Kangaslahti[64], E. Keihänen[19], R. Keskitalo[64,19], T. S. Kisner[72], R. Kneissl[34,5], L. Knox[23], M. Krassenburg[38], H. Kurki-Suonio[19,40], G. Lagache[54], A. Lähteenmäki[1,40], J.-M. Lamarre[67], A. E. Lange[52], A. Lasenby[4,66], R. J. Laureijs[38], C. R. Lawrence[64], S. Leach[80], J. P. Leahy[65], R. Leonardi[36,38,24], C. Leroy[54,89,9], P. B. Lilje[60,11], M. Linden-Vørnle[14], M. López-Caniego[62], S. Lowe[65], P. M. Lubin[24], J. F. Macías-Pérez[70], T. Maciaszek[7], C. J. MacTavish[66], B. Maffei[65], D. Maino[28,46], N. Mandolesi[45], R. Mann[81], M. Maris[44], E. Martínez-González[62], S. Masi[27], M. Massardi[42], S. Matarrese[26], F. Matthai[73], P. Mazzotta[31], A. McDonald[37], P. McGehee[52], P. R. Meinhold[24], A. Melchiorri[27], J.-B. Melin[13], L. Mendes[36], A. Mennella[28,44], C. Mevi[37], R. Miniscalco[37], S. Mitra[64], M.-A. Miville-Deschênes[54,6], A. Moneti[55], L. Montier[89,9], G. Morgante[45], N. Morisset[50], D. Mortlock[51], D. Munshi[82,59], A. Murphy[75], P. Naselsky[76,32], P. Natoli[30,2,45], C. B. Netterfield[16], H. U. Nørgaard-Nielsen[14], F. Noviello[54], D. Novikov[51], I. Novikov[76], I. J. O'Dwyer[64], I. Ortiz[35], S. Osborne[86], P. Osuna[35], C. A. Oxborrow[14], F. Pajot[54], R. Paladini[85,10], B. Partridge[39], F. Pasian[44], T. Passvogel[38], G. Patanchon[3], D. Pearson[64], T. J. Pearson[10,52], O. Perdereau[71], L. Perotto[70], F. Perrotta[80], F. Piacentini[27], M. Piat[3], E. Pierpaoli[18], S. Plaszczynski[71], P. Platania[63], E. Pointecouteau[89,9], G. Polenta[2,43], N. Ponthieu[54], L. Popa[57], T. Poutanen[40,19,1], G. Prézeau[10,64], S. Prunet[55], J.-L. Puget[54], J. P. Rachen[73], W. T. Reach[90], R. Rebolo[61,33], M. Reinecke[73], J.-M. Reix[87], C. Renault[70], S. Ricciardi[45], T. Riller[73], I. Ristorcelli[89,9], G. Rocha[64,10], C. Rosset[3], M. Rowan-Robinson[51], J. A. Rubiño-Martín[61,33], B. Rusholme[52], E. Salerno[8], M. Sandri[45], D. Santos[70], G. Savini[78], B. M. Schaefer[88], D. Scott[17], M. D. Seiffert[64,10], P. Shellard[12], A. Simonetto[63], G. F. Smoot[22,72,3], C. Sozzi[63], J.-L. Starck[68,13], J. Sternberg[38], F. Stivoli[47], V. Stolyarov[4], R. Stompor[3], L. Stringhetti[45], R. Sudiwala[82], R. Sunyaev[73,83], J.-F. Sygnet[55], D. Tapiador[35], J. A. Tauber[38], D. Tavagnacco[44], D. Taylor[35], L. Terenzi[45], D. Texier[35], L. Toffolatti[15], M. Tomasi[28,46], J.-P. Torre[54], M. Tristram[71], J. Tuovinen[74], M. Türler[50], M. Tuttlebee[37], G. Umana[41], L. Valenziano[45], J. Valiviita[60], J. Varis[74], L. Vibert[54], P. Vielva[62], F. Villa[45], N. Vittorio[31], L. A. Wade[64], B. D. Wandelt[55,25], C. Watson[37], S. D. M. White[73], M. White[22], A. Wilkinson[65], D. Yvon[13], A. Zacchei[44], and A. Zonca[24]

(Affiliations can be found after the references)

Received 8 January 2011 / Accepted 31 May 2011

ABSTRACT

The European Space Agency's *Planck* satellite was launched on 14 May 2009, and has been surveying the sky stably and continuously since 13 August 2009. Its performance is well in line with expectations, and it will continue to gather scientific data until the end of its cryogenic lifetime. We give an overview of the history of *Planck* in its first year of operations, and describe some of the key performance aspects of the satellite. This paper is part of a package submitted in conjunction with *Planck*'s Early Release Compact Source Catalogue, the first data product based on *Planck* to be released publicly. The package describes the scientific performance of the *Planck* payload, and presents results on a variety of astrophysical topics related to the sources included in the Catalogue, as well as selected topics on diffuse emission.

Key words. cosmology: observations – cosmic background radiation – surveys – space vehicles: instruments – instrumentation: detectors – catalogs

1. Introduction

The *Planck* satellite[1] was launched on 14 May 2009, and has been surveying the sky stably and continuously since 13 August 2009. *Planck* carries a scientific payload consisting of an array of 74 detectors sensitive to a range of frequencies between ~25 and ~1000 GHz, which scan the sky simultaneously and continuously with an angular resolution varying between ~30 arcmin at the lowest frequencies and ~5 arcmin at the highest. The array is arranged into two instruments: the detectors of the Low Frequency Instrument (LFI; Bersanelli et al. 2010; Mennella et al. 2011) are pseudo-correlation radiometers, covering three bands centred at 30, 44, and 70 GHz; and the detectors of the High Frequency Instrument (HFI; Lamarre et al. 2010; Planck HFI Core Team 2011a) are bolometers, covering six bands centred at 100, 143, 217, 353, 545 and 857 GHz. The design of *Planck* allows it to image the whole sky approximately twice per year, with an unprecedented combination of sensitivity, angular resolution, and frequency coverage. The *Planck* satellite, its payload, and its performance as predicted at the time of launch, are described in 13 articles included in a special issue (Vol. 520) of Astronomy & Astrophysics.

The main objective of *Planck* is to measure the spatial anisotropies of the temperature of the cosmic microwave background (CMB), with an accuracy set by fundamental astrophysical limits. Its level of performance will enable *Planck* to extract essentially all the information in the CMB temperature anisotropies. *Planck* will also measure to high accuracy the polarisation of the CMB anisotropies, which encodes not only a wealth of cosmological information, but also provides a unique probe of the thermal history of the Universe during the time when the first stars and galaxies formed. In addition, the *Planck* sky surveys will produce a wealth of information on the properties of extragalactic sources and on the dust and gas in our own Galaxy. The scientific objectives of *Planck* are described in detail in Planck Collaboration (2005).

At the time this paper is being submitted, *Planck* is close to completing three surveys of the whole sky, and is releasing to the public its first set of scientific data. This data set is the Early Release Compact Source Catalogue (ERCSC), a list of unresolved and compact sources extracted from the first complete all-sky survey carried out by *Planck*. The ERCSC (Planck Collaboration 2011c) consists of:

- nine lists of sources, extracted independently from each of *Planck*'s nine frequency bands;
- two lists of sources extracted using multi-band criteria targetted at selecting specific types of source, i.e.,
  - "Cold Cores," cold and dense locations in the insterstellar medium of the Milky Way, selected mainly based on their estimated dust temperature;
  - clusters of galaxies, selected using the spectral signature left on the CMB by the Sunyaev-Zeldovich (SZ) effect.

The ERCSC is a high-reliability compilation of sources, released early to give the astronomical community a timely opportunity to follow up these sources using ground- or space-based observatories, most particularly ESA's *Herschel* observatory, which has a limited lifetime. The ERCSC is being released by ESA to the public on 11 January 2011 through an online distribution system accessible via `http://www.rssd.esa.int/Planck`. At the same time, the *Planck* Collaboration is submitting for publication a package of consisting of:

- this paper (Planck Collaboration 2011a), which describes the history and main performance elements of the *Planck* satellite in its first year of life;
- two papers describing the performance of each of *Planck*'s two instruments (LFI and HFI) within the same period (Mennella et al. 2011; and Planck HFI Core Team 2011a);
- a paper describing the thermal performance of *Planck* in orbit (Planck Collaboration 2011b);
- two papers describing the data processing, which has been applied to the data acquired by LFI and HFI, to produce the maps used for the ERCSC and the scientific papers in this package (Zacchei et al. 2011; and Planck HFI Core Team 2011b);
- an Explanatory Supplement to the ERCSC (Planck Collaboration 2011v), describing in detail the production and characteristics of the ERCSC;
- a paper summarising the production of the ERCSC, and the main characteristics of the sources that it contains (Planck Collaboration 2011c);
- twelve papers describing in more detail: (a) specific aspects of different source populations contained in the ERCSC (radio sources, infrared galaxies, galaxy clusters, cold cores etc.); and (b) cross-correlation analysis and follow-up observations which form part of the scientific validation and analysis of the ERCSC data. These papers are:
  1. Planck Collaboration (2011d) describes the physical properties of the sample of clusters included in the ERCSC;
  2. Planck Collaboration (2011e) describes the validation of a subset of the cluster sample by follow-up observations with the *XMM-Newton* X-ray observatory;
  3. Planck Collaboration (2011f) analyses the statistical relationship between SZ flux and X-ray luminosity of the ERCSC cluster sample;
  4. Planck Collaboration (2011g) uses a high signal-to-noise subset of the ERCSC cluster sample to investigate the relationship between X-ray-derived masses and SZ fluxes;
  5. Planck Collaboration (2011h) studies the relation between SZ flux and optical properties of galaxy clusters by stacking *Planck* fluxes at the locations of the MaxBCG optical cluster catalogue;
  6. Planck Collaboration (2011w) studies an exceptionally X-ray luminous and massive galaxy cluster detected by *Planck* at $z \sim 1$;
  7. Planck Collaboration (2011i) analyses the statistical properties of a complete sub-sample of radio sources drawn from the ERCSC;
  8. Planck Collaboration (2011j) describes the spectral energy distributions and other properties of some extreme radio sources, using *Planck* ERCSC data and ground-based observations;
  9. Planck Collaboration (2011k) presents the spectral energy distributions of a sample of extragalactic radio sources, based on the *Planck* ERCSC and simultaneous multi-frequency data from a range of other observatories;

⋆ Corresponding author: J. A. Tauber,
e-mail: `jtauber@rssd.esa.int`

[1] *Planck* (`http://www.esa.int/Planck`) is a project of the European Space Agency – ESA – with instruments provided by two scientific Consortia funded by ESA member states (in particular the lead countries: France and Italy) with contributions from NASA (USA), and telescope reflectors provided in a collaboration between ESA and a scientific Consortium led and funded by Denmark.

10. Planck Collaboration (2011l) studies the dust properties of nearby galaxies ($z < 0.25$) present in the ERCSC;
11. Planck Collaboration (2011s) presents the statistical properties of Cold Cores as observed by *Planck*, in terms of spatial distribution, temperature, distance, mass, and morphology;
12. Planck Collaboration (2011r) presents the physical properties and discusses the nature of a selection of interesting Cold Cores observed by *Planck*.

– seven papers describing in more detail selected science results, based on the maps which were used as input for the production of the ERCSC. The results addressed in these papers are characterised by their robustness, a critical element required for publication at a rather early stage in the reduction of the *Planck* data. These seven are:
  1. Planck Collaboration (2011m) presents estimates based on *Planck* and *IRAS* data for the apparent temperature and optical depth of interstellar dust in the Small and Large Magellanic Clouds, and investigates the nature of the millimetre-wavelength excess emission observed in these galaxies;
  2. Planck Collaboration (2011n) presents estimates of the angular power spectrum of the cosmic infrared background as observed by *Planck* in selected regions of the sky;
  3. Planck Collaboration (2011o) estimates over the whole sky the apparent temperature and optical depth of interstellar dust based on *Planck* and *IRAS* data, and investigates the presence of "dark" gas, i.e., gas which is not spatially correlated with known tracers of neutral and molecular gas;
  4. Planck Collaboration (2011p) constructs the spectral energy distributions of selected regions in the Milky Way, using *Planck* maps combined with ancillary multi-frequency data, and investigates the presence of anomalous excess emission which can be interpreted as arising from small spinning grains;
  5. Planck Collaboration (2011q) estimates the radial distribution of molecular, neutral, and ionised gas in the Milky Way, using as spatial templates a wide variety of tracers of the different phases and components of the interstellar medium;
  6. Planck Collaboration (2011t) presents a joint analysis of *Planck*, *IRAS*, and 21-cm observations of selected high-Galactic-latitude fields, and discusses the properties of dust in the diffuse interstellar medium close to the Sun and in the Galactic halo;
  7. Planck Collaboration (2011u) presents *Planck* maps of a selection of nearby molecular clouds, and discusses the evolution of the emitting properties of the dust particles embedded in them.

The next release of *Planck* products will take place in January 2013, and will cover data acquired in the period up to 27 November 2010. It will include:

– cleaned and calibrated data timelines for each detector;
– maps in Stokes I, Q, and U for each frequency band between 30 and 353 GHz, and in Stokes I for the two highest frequency bands (545 and 857 GHz);
– catalogues of compact sources extracted from the frequency maps;
– maps of the main diffuse components separated from the maps, including the CMB;
– scientific results based on the data released.

A third release of products is foreseen after January 2014, to cover the data acquired beyond November 2010 and the end of *Planck* operations.

This paper is mainly dedicated to describing the history of the mission from launch until 6 June 2010 (the coverage period of the data used to generate the ERCSC). It also discusses some performance aspects of the satellite which are important for the interpretation of its scientific output. It serves therefore as background and reference for the suite of papers described above. In Sects. 2 and 3, we describe the main events and activities which took place before the start of the *Planck* surveys. In Sect. 4, we describe relevant aspects of the *Planck* surveys, i.e., the strategy used to scan the sky, its thermal and radiation environment, the pointing performance of the satellite, and the flow of data in the ground segment. Finally, in Sect. 5 we summarise the scientific performance of the payload as estimated from the first year of data and with the current set of available data processing pipelines.

2. Early operations and transfer to orbit

Planck was launched from the Centre Spatial Guyanais in Kourou (French Guyana) on 14 May 2009 at its nominal lift-off time of 13:12 UT, on an Ariane 5 ECA rocket of Arianespace[2]. ESA's *Herschel* observatory was launched on the same rocket. At 13:37:55 UT, *Herschel* was released from the rocket at an altitude of 1200 km; *Planck* followed suit at 13:40:25 UT. The separation attitudes of both satellites were within $0.^{\circ}1$ of prediction. The Ariane rocket placed *Planck* with excellent accuracy (semi-major axis within 1.6% of prediction), on a trajectory towards the second Lagrangian point of the Earth-Sun system ("L_2") which is drawn in Fig. 1. The orbit describes a Lissajous trajectory around L_2 with a ~6 month period that avoids crossing the Earth penumbra for at least 4 years.

After release from the rocket, three large manoeuvres were carried out to place *Planck* in its intended final orbit. The first (14.35 m s^{-1}), intended to correct for errors in the rocket injection, was executed on 15 May at 20:01:05 UT, with a slight overperformance of 0.9% and an error in direction of $1.^{\circ}3$ (a touch-up manoeuvre was carried out on 16 May at 07:17:36 UT). The second and major (mid-course) manoeuvre (153.6 m s^{-1}) took place between 5 and 7 June, and a touch-up (11.8 m s^{-1}) was executed on 17 June. The third and final manoeuvre (58.8 m s^{-1}), to inject *Planck* into its final orbit, was executed between 2 and 3 July. The total fuel consumption of these manoeuvres, which were carried out using *Planck*'s coarse (20 N) thrusters, was 205 kg. Once in its final orbit, very small manoeuvres are required at approximately monthly intervals (1 m s^{-1} per year) to keep *Planck* from drifting away from its intended path around L_2. The attitude manoeuvres required to follow the scanning strategy require about 2.6 m s^{-1} per year. Overall, the excellent performance of launch and orbit manoeuvres will lead to a large amount (~160 kg, or ~40% of initial tank loading) of fuel remaining on board at end of mission operations.

Planck started cooling down radiatively shortly after launch. Heaters were activated to hold the focal plane at 250 K, which was reached around 5 h after launch. The valve opening the exhaust piping of the dilution cooler was activated at 03:30 UT, and the ^{4}He-JT cooler compressors were turned on at low stroke at 05:20 UT. After these essential operations were completed, on the second day after launch, the focal plane temperature was

[2] More information on the launch facility and the launcher are available at http://www.arianespace.com

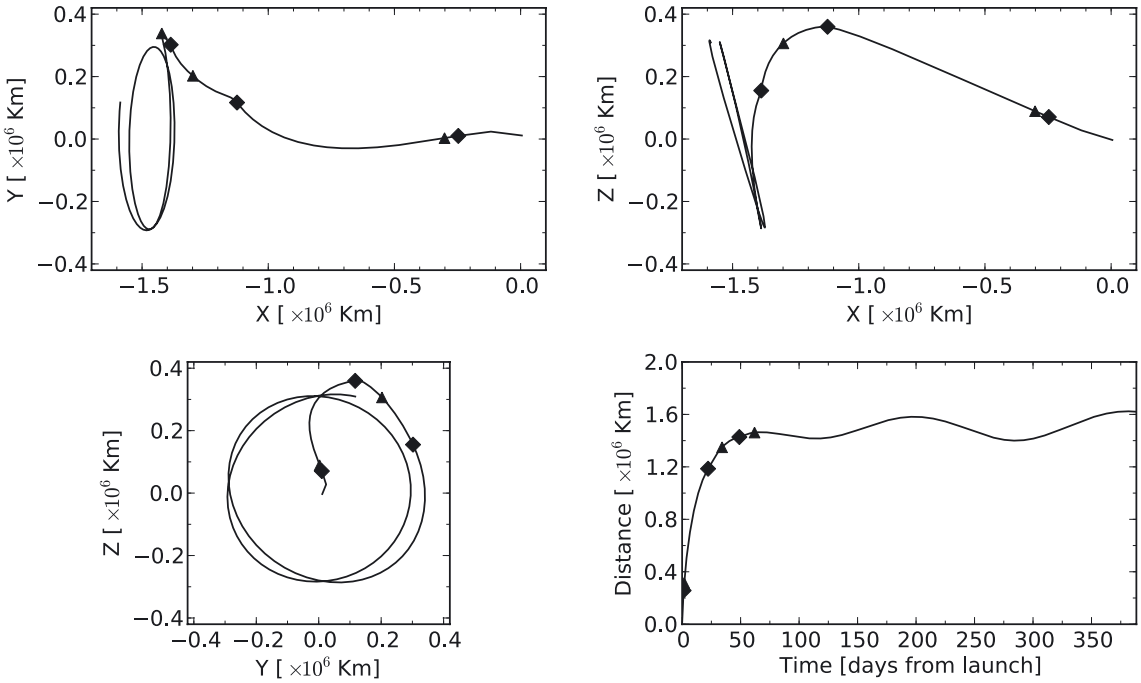

Fig. 1. The trajectory of *Planck* from launch until 6 June 2010, in Earth-centred rotating coordinates (X is in the Sun-Earth direction, and Z points to the north ecliptic pole). Diamond symbols indicate the major manoeuvres, while triangles are touch-up operations. Two orbits around L_2 have been carried out in this period. The orbital periodicity is ~6 months. The distance from the Earth-Moon barycentre is shown at *bottom right*.

allowed to descend to 170 K for out-gassing and decontamination of the telescope and focal plane.

3. Commissioning and initial science operations

The first period of operations focussed on commissioning activities, i.e., functional check-out procedures of all sub-systems and instruments of the *Planck* spacecraft in preparation for running science operations related to calibration and performance verification of the payload. Planning for commissioning operations was driven by the telescope decontamination period of 2 weeks and the subsequent cryogenic cool-down of the payload and instruments. The overall duration of the cool-down was approximately 2 months, including the decontamination period.

The sequence of commissioning activities covered the following areas:

- on-board commanding and data management;
- attitude measurement and control;
- manoeuvreing ability and orbit control;
- telemetry and telecommand;
- power control;
- thermal control;
- payload basic functionality, including:
  - the LFI;
  - the HFI;
  - the cryogenic chain;
  - the Standard Radiation Environment Monitor (SREM, see Sect. 4.4);
  - the Fibre-Optic Gyro unit (FOG), a piggy-back experiment which is not used as part of the attitude control system.

The commissioning activities were executed very smoothly and all sub-systems were found to be in good health. Figure 2 shows a sketch of the cool-down sequence indicating when the main instrument-related commissioning activities took place. The most significant unexpected issues that had to be addressed during these early operational phases were the following.

- The X-band transponder showed an initialisation anomaly during switch-on which was fixed by a software patch.
- Large reorientations of the spin axis were imperfectly completed and required optimisation of the on-board parameters of the attitude control system.
- The data rate required to transmit all science data to the ground was larger than planned, due to the unexpectedly high level of Galactic cosmic rays (see Sect. 4.4), which led to a high glitch rate on the data stream of the HFI bolometers (Planck HFI Core Team 2011a); glitches increase the dynamic range and consequently the data rate. The total data rate was controlled by increasing the compression level of a few less critical thermometers.
- The level of thermal fluctuations in the 20-K stage was higher than originally expected. Optimisation of the sorption cooler operation led to an improvement, though they still remained ~25% higher than expected (Planck Collaboration 2011b).
- The 20-K sorption cooler turned itself off on 10 June 2009, an event which was traced to an incorrectly set safety threshold.
- A small number of sudden pressure changes were observed in the ^{4}He-JT cooler during its first weeks of operation, and were most likely due to impurities present in the cooler gas (Planck Collaboration 2011b). The events disappeared after some weeks, as the impurities became trapped in the cooler system.
- The ^{4}He-JT cooler suffered an anomalous switch to standby mode on 6 August 2009, following a current spike in the charge regulator unit which controls the current levels between the cooler electronics and the satellite power supply (Planck Collaboration 2011b). The cooler was restarted 20 h

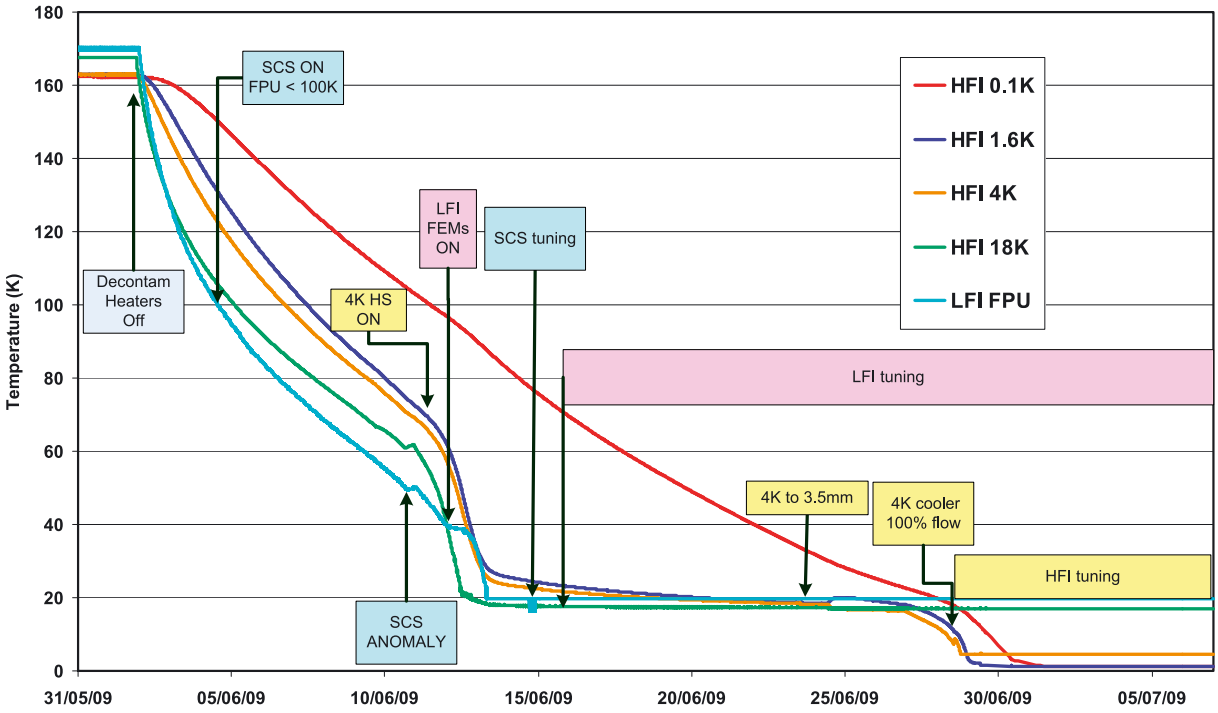

Fig. 2. A sketch of the cool-down sequence, indicating when the main instrument and cryo-chain-related activities took place in the early phases of the mission. The coloured curves trace the temperature of each stage in the cryogenic chain. The arrows indicate some of the key events in the sequence, as described in the text. (Note: SCS = sorption cooler system; FEM = LFI front-end modules; FPU = focal plane unit; and HS = heat switch.) The events are colour-coded by sub-system: blue for the sorption cooler; pink for LFI; and yellow for HFI. "LFI tuning" refers mainly to the optimisation of the bias settings of the FEMs, whereas "HFI tuning" refers mainly to optimisation of the thermal control loops at each low-temperature stage.

after the event, and the thermal stability of the 100-mK stage was recovered about 47 h later. The physical cause of this anomaly was not found, but the problem has not recurred.
- Instabilities were observed in the temperature of the ^{4}He-JT stage, which were traced to interactions with lower temperature stages, similar in nature to instabilities observed during ground testing (Planck Collaboration 2011b). They were fixed by exploring and tuning the operating points of the multiple stages of the cryo-system.
- The length of the daily telecommunications period was increased from 180 to 195 min to improve the margin available and ensure completion of all daily activities[3].

The commissioning activities were formally completed at the time when the HFI bolometer stage reached its target temperature of 100 mK, on 3 July 2009 at 01:00 UT. At this time all the critical resource budgets (power, fuel, lifetime, etc.) were found to contain very significant margins with respect to the original specification.

Calibration and performance verification (CPV) activities started during the cool-down period and continued until the end of August 2009. Their objectives were to:

- verify that the instruments were optimally tuned and their performance characterised and verified;
- perform all tests and characterisation activities which could not be performed during the routine phase;
- characterise the spacecraft and telescope characteristics of relevance for science[4];
- estimate the lifetime of the cryogenic chain.

CPV activities addressed the following areas:

- tuning and characterisation of the behaviour of the cryogenic chain;
- characterisation of the thermal behaviour of the spacecraft and payload;
- for each of the two instruments: tuning; characterisation and/or verification of performance[5], calibration (including thermal, RF, noise and stability, optical response); and data compression properties;
- determination of the focal plane footprint on the sky;
- verification of scanning strategy parameters;
- characterisation of systematic effects induced by the spacecraft and the telescope, including:
  - dependence on solar aspect angle;
  - dependence on spin;
  - interference from the RF transmitter;
  - straylight rejection;
  - pointing performance.

The schedule of CPV activities consumed about two weeks longer than initially planned, mainly due to:

[3] Subsequent optimisations of operational procedures allowed the daily contact period to be reduced again to 3 h.

[4] Detailed optical characterisation requires the observation of planets, which first came into the field-of-view in October 2009, i.e., after the start of routine operations.

[5] In the case of LFI, an optimisation of the detector parameters was carried out in-flight (Mennella et al. 2011), whereas for HFI, it was merely verified that the on-ground settings had not changed (Planck HFI Core Team 2011a).

- the anomalous switch to standby mode of the ^{4}He-JT cooler on 6 August (costing 6 days until recovery);
- instabilities in the cryo-chain, which required the exploration of a larger parameter phase space to find an optimal setting point;
- additional measurements of the voltage bias space of the LFI radiometers, which were introduced to optimise its noise performance, and led to the requirement of artificially slowing the natural cool-down of the ^{4}He-JT stage.

A more detailed description of the relevant parts of these tests can be found in Mennella et al. (2011) and Planck HFI Core Team (2011a). On completion of all the planned activities, it was concluded that:

- the two instruments were fully tuned and ready for routine operations. No further parameter tuning was expected to be needed, except for the sorption cooler, which requires a weekly change in operational parameters (Planck Collaboration 2011b);
- the scientific performance parameters of both instruments was in most respects as had been measured on the ground before launch. The only significant exception was that, due to the high level of Galactic cosmic rays, the bolometers of HFI were detecting a higher number of glitches than expected, causing a modest (~10%) level of systematic effects on their noise properties (see details in Planck HFI Core Team 2011a);
- the telescope survived launch and cool-down in orbit without any major distortions or changes in its alignment;
- the lifetime of the cryogenic chain was adequate to carry the mission to its foreseen end of operations in November 2010, with a margin of order one year;
- the pointing performance was better than expected, and no changes to the planned scanning strategy were required;
- the satellite did not introduce any major systematic effects into the science data. In particular, the telemetry transponder did not result in radio-frequency interference, which implies that the data acquired during visibility periods is useable for science.

The First Light Survey (FLS) was the last major activity planned before the start of routine surveying of the sky. It was conceived as a two-week period during which *Planck* would be fully tuned up and operated as if it was in its routine phase. This stable period could have resulted in the identification of further tuning activities required to optimise the performance of *Planck* in the long-duration surveys to come. The FLS was conducted between 13 and 27 August, and in fact led to the conclusion that the *Planck* payload was operating stably and optimally, and required no further tuning of its instruments. Therefore the period of the FLS was accepted as a valid part of the first *Planck* survey.

4. Routine operations phase

The routine operations phase of *Planck* is characterised by continuous and stable scanning of the sky and data acquisition by LFI and HFI. It started with the FLS on 13 August of 2009, at 14:15 UT. In this section we describe the major characteristics of this phase from start until 6 June 2010, i.e., the period over which data were used to generate the ERCSC.

4.1. Mission operations and data flow

A general description of mission operations is provided in Tauber et al. (2010a).

The *Planck* satellite generates (and stores on-board) data continuously at the following typical rates: 21 kilobit s^{-1} (kbps) of house-keeping (HK) data from all on-board sources, 44 kbps of LFI science data and 72 kbps of HFI science data. The data are brought to ground in a daily pass of approximately 3 h duration. Besides the data downloads, the passes also acquire real-time HK and a 20 min period of real-time science (used to monitor instrument performance during the pass). *Planck* utilises the two ESA deep-space ground stations in New Norcia (Australia) and Cebreros (Spain), usually the former. Scheduling of the daily telecommunication period is quite stable, with small perturbations due to the need to coordinate the use of the antenna with other ESA satellites (in particular *Herschel*).

At the ground station the telemetry is received by redundant chains of front-end/back-end equipment. The data flows to the mission operations control centre (MOC) located at ESOC in Darmstadt (Germany), where it is processed by redundant mission control software (MCS) installations and made available to the science ground segment. To reduce bandwidth requirements between the station and ESOC only one set of science telemetry is usually transferred. Software is run post-pass to check the completeness of the data. This software check is also used to build a catalogue of data completeness, which is used by the science ground segment to control its own data transfer process. Where gaps are detected, attempts to fill them are made as an offline activity (normally next working day), the first step being to attempt to reflow the relevant data from station. Early in the mission these gaps were more frequent, with some hundreds of packets affected per week (impact on data return of order 50 ppm) due principally to a combination of software problems with the data ingestion and distribution in the MCS, and imperfect behaviour of the software gap check. Software updates implemented during the mission have improved the situation such that gaps are much rarer, with a total impact on data return well below 1 ppm.

Redump of data from the spacecraft is attempted when there have been losses in the space link. This has only been necessary on three occasions. In each case the spacecraft redump has successfully recovered all the data.

An operational principle of the mission is to avoid impact on the nominal science of a completely missed ground station pass. Commanding continuity is managed by keeping more than 24 h of commanding-timeline queued on-board. The telemetry resides on board the satellite in a ~60 h circular buffer in solid-state memory, and can be recovered subsequently using the margin in each pass, or more rapidly by seeking additional station coverage after an event. The lost-pass scenario has in fact occurred only once (on 21 December 2009), when snow on the dish at Cebreros led to the loss of the entire pass. A rapid recovery was made by using spare time available on the New Norcia station. Smaller impacts on the pass occur more often (e.g., the first ~10 min of a pass may be lost due to a station acquisition problem) and these can normally be recovered simply by restarting a software task or rebooting station equipment. Such delays are normally accommodated within the margin of the pass itself, or during the subsequent pass.

All the data downloaded from the satellite, and processed products such as filtered attitude information, are made available each day for retrieval from the MOC by the LFI and HFI Data Processing Centres (DPCs). Typically, the data arrive at

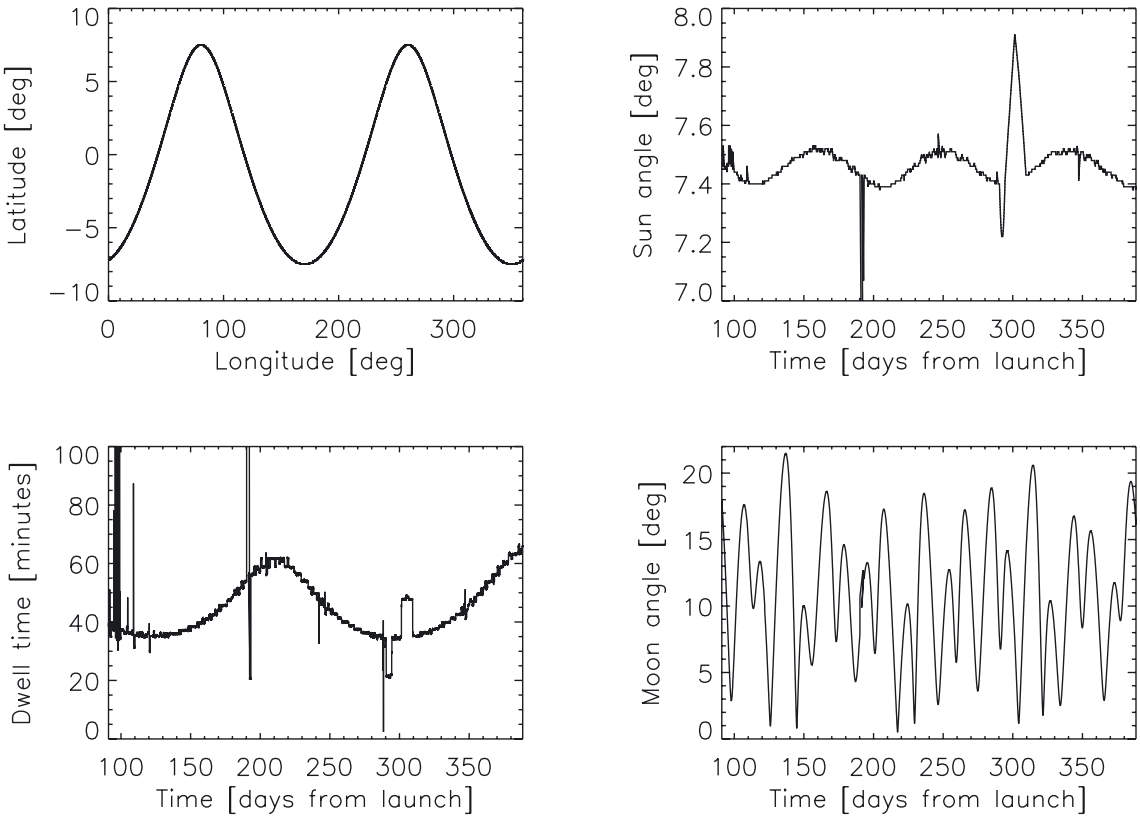

Fig. 3. *Top left*: the path of the spin axis of *Planck* (in Ecliptic latitude and longitude) over the period 13 August 2009 to 6 June 2010. The evolution of the dwell time (bottom left) and of the solar aspect angle (i.e. the angle between the anti-Sun direction and the spin axis, *top right*) are shown during the same period. The "day *Planck* stood still" (day 191) and the period of acceleration/deceleration during observations of the Crab (between days 291 and 310) are clearly visible in both plots. *Bottom right*: the evolution of the angle between the Moon and the anti-spin axis.

Table 1. *Planck* coverage statistics.

	30 GHz	100 GHz	545 GHz	
Mean[a]	2293	4575	2278	s deg^{-2}
Minimum	440	801	375	s deg^{-2}
<half Mean[b]	14.4	14.6	15.2	%
>4 × Mean[c]	1.6	1.5	1.2	%
>9 × Mean[d]	0.41	0.42	0.41	%

Notes. [(a)] Mean over the whole sky of the integration time cumulated for all detectors (definition as in Table 3) in a given frequency channel. [(b)] Fraction of the sky whose coverage is less than half the Mean. [(c)] Fraction of the sky whose coverage is larger than four times the Mean. [(d)] Fraction of the sky whose coverage is larger than nine times the Mean.

the LFI (resp. HFI) DPC 2 (resp. 4) hours after the start of the daily acquisition window. Automated processing of the incoming telemetry is carried out each day by the LFI (resp. HFI) DPCs and yields a daily data quality report which is made available to the rest of the ground segment typically 22 (resp. 14) hours later. More sophisticated processing of the data in each of the two DPCs is described in Zacchei et al. (2011) and Planck HFI Core Team (2011b).

4.2. Scanning strategy

The strategy used to scan the sky is described in Tauber et al. (2010a). The spin axis follows a cycloidal path on the sky as shown in Fig. 3, by step-wise displacements of 2 arcmin approximately every 50 min. The dwell time (i.e., the duration of stable data acquisition at each pointing) has varied sinusoidally by a factor of ∼2 (see Fig. 3). *Planck*'s scanning strategy results in significantly inhomogeneous depth of integration time across the sky; the areas near the ecliptic poles are observed with greater depth than all others. This is illustrated in Figs. 4 and 5. Table 1 shows more quantitatively the coverage of the sky at three representative frequencies.

The major pre-planned deviation from the nominal spin axis path took place in the period 1 to 19 March 2010. During this time, the average daily progression speed of the spin axis (normally 1 deg day^{-1}) was temporarily increased, to gain a margin with respect to the attitude constraints imposed by the Sun and the Earth at the time that the Crab Nebula, *Planck*'s main polarisation calibrator, was being observed. This increased margin would have allowed *Planck* to re-observe the Crab if a significant problem had been encountered, but none occurred. A corresponding deceleration was included to rejoin the normal scanning path after the Crab had been observed by all detectors. The whole operation (clearly visible in Fig. 3) also resulted in a deviation of the solar aspect angle.

Orbit maintenance manoeuvres were carried out at approximately monthly intervals[6]. Although the manoeuvres only required a few minutes, preparations, post-manoeuvre mass-property calibration, and re-entry into scientific slewing mode increased the overhead to several hours. The manoeuvres were carried out without disturbing the path of the spin axis from its

[6] On 14 August 2009, 11 September 2009, 04 December 2009, 15 January 2010, 26 February 2010, and 26 March 2010.

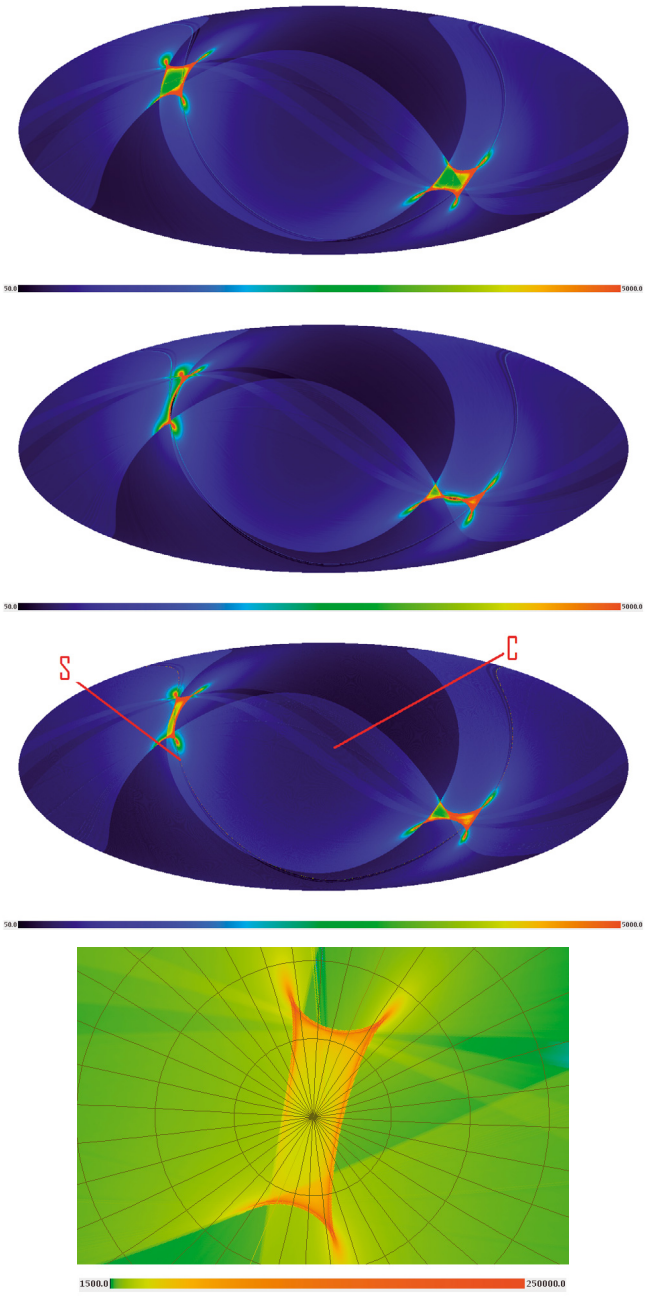

Fig. 4. Survey coverage (the colour scale represents integration time varying between 50 and 5000 s deg^{-2}) for three individual detectors located near the edges (LFI-24 and LFI-25 at 44 GHz, *top panels*) and centre of the focal plane HFI 353-1 at 353 GHz, *third panel*). The maps are Mollweide projections of the whole sky in Galactic coordinates, pixelised according to the Healpix (Górski et al. 2005) scheme at $N_{\rm side}$ = 1024. The features due to "the day Planck stood still" and the Crab slow-down (Sect. 4.2) are pointed out as "S" and "C" respectively. *The bottom panel* is a zoom on the area around the North Ecliptic Pole, showing (in logarithmic scale) the distribution of high sensitivity observations integrated for all 100 GHz detectors.

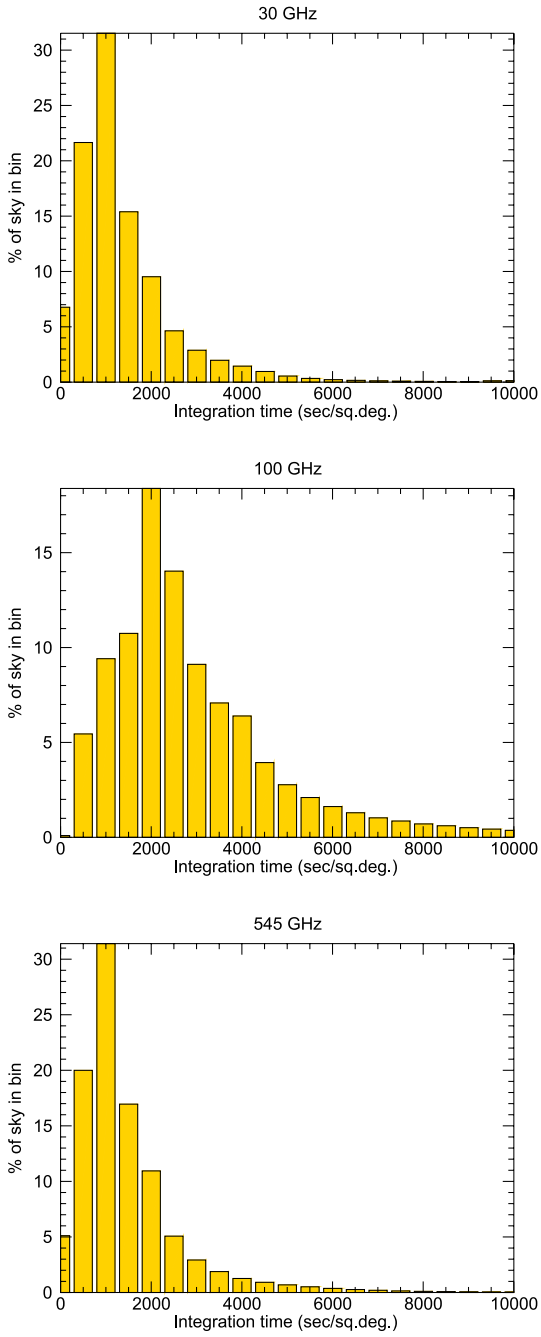

Fig. 5. Histograms of integration time (in s deg^{-2}) cumulated for all detectors at 30 GHz (*top panel*), 100 GHz (*middle panel*), and 545 GHz (*bottom panel*). Characteristic coverage quantities are listed in Table 1.

nominal scanning law. The dwell times of pointings before and after the execution of the manoeuvre were reduced to allow all pre-planned pointings to be carried out.

The main unplanned deviations from the basic scanning strategy included the following.

– An operator error in the upload of the on-board command timeline led to an interruption of the normal sequence of manoeuvres and therefore to *Planck* pointing to the same location on the sky for a period of 29 h between 20 and 21 November 2009 ("the day *Planck* stood still"). Observations of the nominal scanning pattern resumed on 22 November, and on 23 November a recovery operation was applied to survey the previously missed area. During the recovery period the duration of pointing was decreased to allow the nominal law to be caught up with. As a side effect, the RF transmitter was left on for longer than 24 h, which had a significant thermal impact on the warm part of the satellite (see Fig. 6).

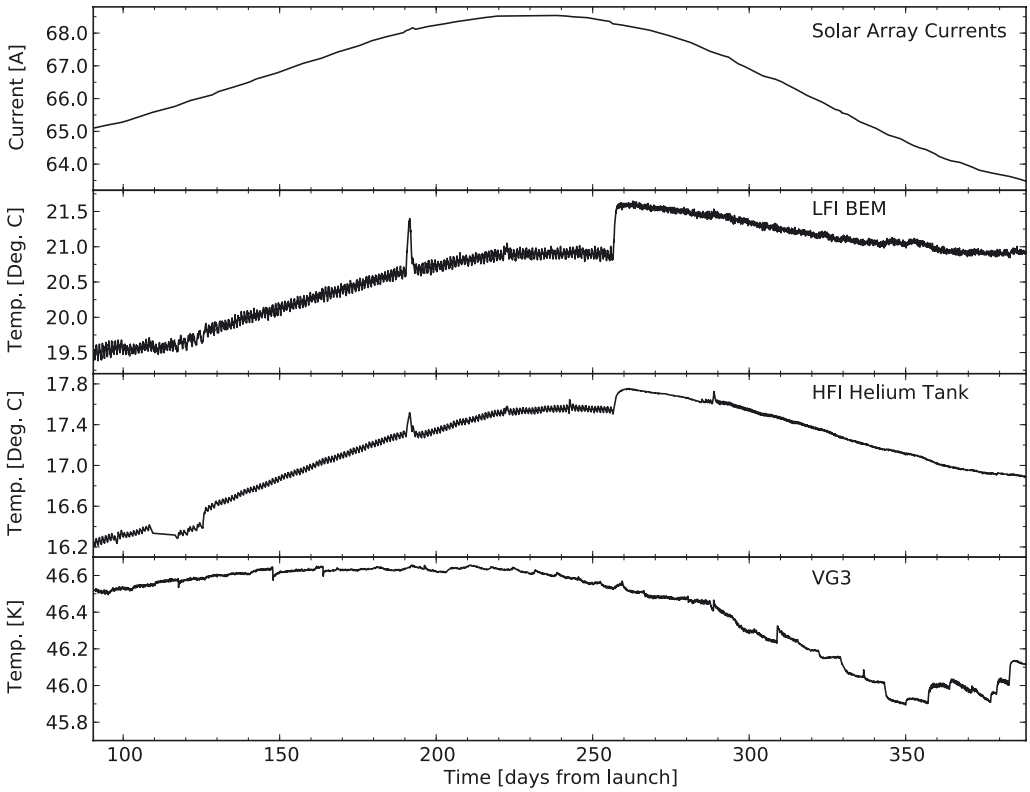

Fig. 6. The main long-timescale thermal modulation is a seasonal effect driven by the solar power absorbed by the satellite. The evolution of the solar heat input is traced by the top figure which shows the total current produced by the solar panels; the long-term variation is largely a reflection of the distance from the Sun, with a very small modulation due to variations in the satellite's aspect angle to the Sun. *The top and second panels* show the temperature variation at two representative locations in the room-temperature service module (SVM), i.e., on one of the (HFI) helium tanks and on one of the LFI back-end modules (BEM). *The bottom panel* shows the temperature evolution of VG3, the coldest of three stacked conical structures or V-grooves which radiatively isolate the warm SVM from the cold payload module. The seasonal effect is not dominant in the evolution of VG3, demonstrating the high thermal isolation of the payload from the SVM. Most variations on VG3 are due to weekly power input adjustments of the sorption cooler (see also Fig. 7), which is heat-sunk to VG3. The main operational disturbances during the routine phase which had a thermal impact can be seen in *the middle two panels* (see text for more detail): **a)** the "catbed" event between 110 and 126 days after launch; **b)** the "day *Planck* stood still" 191 days after launch; **c)** the change in temperature and its daily variation starting 257 days after launch, due to the RF transmitter being turned permanently on; and **d)** two star-tracker reconfiguration events, 242 and 288 days after launch.

- Very minor deviations from the scanning law include occasional (on the average about once every two months) under-performance of the 1-N thrusters used for regular manoeuvres, which implied the corresponding pointings were not at the intended locations. These deviations, visible in Fig. 12, had typical amplitudes of 30″, and have no significant impact on the coverage map.
- During the coverage period, the operational star tracker switched autonomously to the redundant unit on two occasions (11 January 2010 and 26 February 2010); the nominal star tracker was restored a short period later (3.37 and 12.75 h, respectively) by manual power-cycling. Although the science data taken during this period have normal quality, they have not been used because the redundant star tracker's performance is not fully characterised.

While the *Planck* detectors are scanning the sky, they also naturally observe celestial calibrators. The main objects used for this purpose are:

- the Crab Nebula, used to calibrate polarisation properties of the detectors, was observed in September 2009, March 2010 and September 2010;
- the brighter planets, used to map individual detector beams:
  - Jupiter, observed in October 2009 and July 2010;
  - Saturn, observed in January 2010 and June 2010;
  - Mars, observed in October 2009 and April 2010.

The use of these observations for beam and time response calibration is described in Zacchei et al. (2011) and Planck HFI Core Team (2011b).

The scanning strategy for the second year of Routine Operations (i.e., Surveys 3 and 4) is exactly the same as for the first year, except that all pointings are shifted by 1 arcmin along the cross-scanning direction, in order to provide finer sky sampling for the highest frequency detectors when combining two years of observations.

4.3. Thermal environment

The satellite design and its location at L_2 provide an extremely stable thermal environment (see Figs. 6 and 7). The main temperature variation on long timescales is driven by the total radiative power absorbed by the solar panels, which varies depending on distance from the Sun and the solar aspect angle (i.e. the angle between the solar direction and the spin axis). On shorter timescales, temperature variations are driven by active thermal regulation cycles. Both seasonal and shorter-timescale variations are observed across the satellite's service module (SVM), but are heavily damped and almost unobservable within the payload module (PLM).

Specific operations and deviations from the scanning strategy have a thermal influence on the satellite and payload. Some significant effects are clearly visible in Fig. 6 and listed below.

- The thruster heaters were unintentionally turned off between 31 August and 16 September 2009 (the so-called "catbed" event).
- As planned, the RF transmitter was initially turned on and off every day in synchrony with the daily visibility window, in order to reduce potential interference by the transmitter on the scientific data. The induced daily temperature variation had a measurable effect throughout the satellite. An important effect was on the temperature of the ^{4}He-JT cooler compressors, which caused variations of the levels of the interference lines that they induce on the bolometer data (Planck HFI Core Team 2011a). Therefore the RF transmitter was left permanently on starting from 25 January 2010 (257 days after launch), which made a noticeable improvement on the daily temperature variations (Fig. 7).
- A significant thermal effect arises from the (approximately) weekly adjustments to the operation of the Sorption Cooler (Fig. 7).

The thermal environment of the payload module is – by design – extremely well decoupled from that of the service module (Fig. 6). As a consequence, in spite of the significant thermal perturbations originating in the SVM, the thermal variability affecting the detectors is essentially completely due to the operation of the cryogenic cooling chain (described in detail in Planck Collaboration 2011b), which ensures their cold environment.

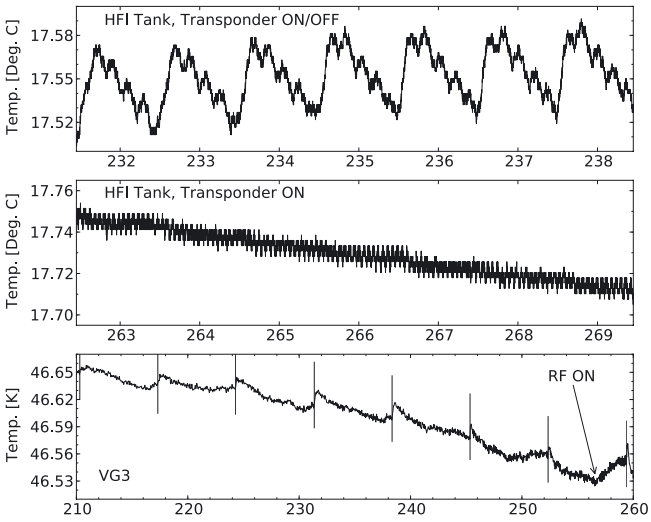

Fig. 7. A zoom of a seven day period on the temperature of a helium tank is shown before (*top panel*) and after (*middle panel*) the RF transponder was left permanently on (see also Fig. 7), and illustrates the reduction in the daily temperature variations achieved by this operation. Smaller variations remain, due to thermal cycling of other elements (in this case the LFI Data Processing Unit), and are clearly visible in *the middle panel*. *The bottom panel* shows the typical effect of weekly updates of the operational parameters of the Sorption Cooler (marked as vertical lines) on the temperature of the third V-groove.

4.4. Radiation environment

The Standard Radiation Environment Monitor on board *Planck* (SREM, Buehler et al. 1996) is a particle detector which is being flown on several ESA satellites. The SREM consists of several detectors sensitive to different energy ranges, which can also be used in coincidence mode. In particular, the SREM measures count rates of high energy protons (from ~10 MeV to ~300 MeV) and electrons (~300 keV to ~6 MeV).

Particle fluxes measured by the SREM on board *Planck* are shown in Fig. 8. The radiation environment of *Planck* is characterised by the current epoch near the minimum in the solar cycle. As a consequence, the particle flux is dominated by Galactic cosmic rays, rather than by the solar wind. The time evolution of the SREM measurements is well correlated with that of identical units flying simultaneously on other satellites (e.g., *Herschel, Rosetta*) and with indicators of Galactic cosmic rays, and is anti-correlated with solar flare events and with the solar cycle (Fig. 8). More importantly for *Planck*, the SREM measurements are very well correlated with the heat deposition on the coldest stages of the HFI, and with glitch rates measured by the detectors of HFI. A more detailed interpretation of these data is provided in Planck HFI Core Team (2011a).

4.5. Pointing performance

Redundant star trackers on board *Planck* (co-aligned within 0.°2 with the instrument field-of-view) provide absolute attitude measurements at a frequency of 8 Hz. These measurements are used by the attitude control computer on board *Planck* to execute the commanded reorientations of the satellite. The star tracker data are further processed on the ground on a daily basis, to provide:

- filtered attitude information at a frequency of 4 Hz during the stable observation periods. The filtering algorithm basically suppresses high-frequency components of the measurement noise (i.e., at frequencies well above the nutation frequency);
- reconstructed attitude parameters averaged over each spin period (60 s) and each stable observation period (or dwell, typically of 50 min length).

The daily filtered attitude information is used by the data processing centres to estimate the location of each detector beam with respect to the satellite reference frame, based mainly on observations of planets (as described in Planck HFI Core Team 2011a). The attitude data during the periods that the satellite is slewing are not filtered on the ground and are therefore much noisier.

Planck rotates about its principal axis of inertia at 1 rpm, with a precision of ±0.1% (see Fig. 9). The observed variation of the spin rate is very systematic due to the following operational features.

- The thruster used for a manoeuvre is selected depending on whether the spin rate preceding the manoeuvre is below or above its nominal value. Each thruster has a slightly different "minimum thrust level", which determines the spin rate actually achieved. Therefore, the spin rate after each manoeuvre will toggle between two different spin rate states which bound the nominal value. If one of these states is very close to the nominal value, drift during the dwell period (see next item) could cause it to change from one side to the other of the nominal value, and thus to toggle on the next manoeuvre to a "third" spin rate state.
- Within a dwell period, the spin rate drifts slightly (typically 10^{-6} deg s^{-1} per minute) due to residual torques on the satellite, caused by solar radiation pressure and exhaust of helium from the dilution cooler system.

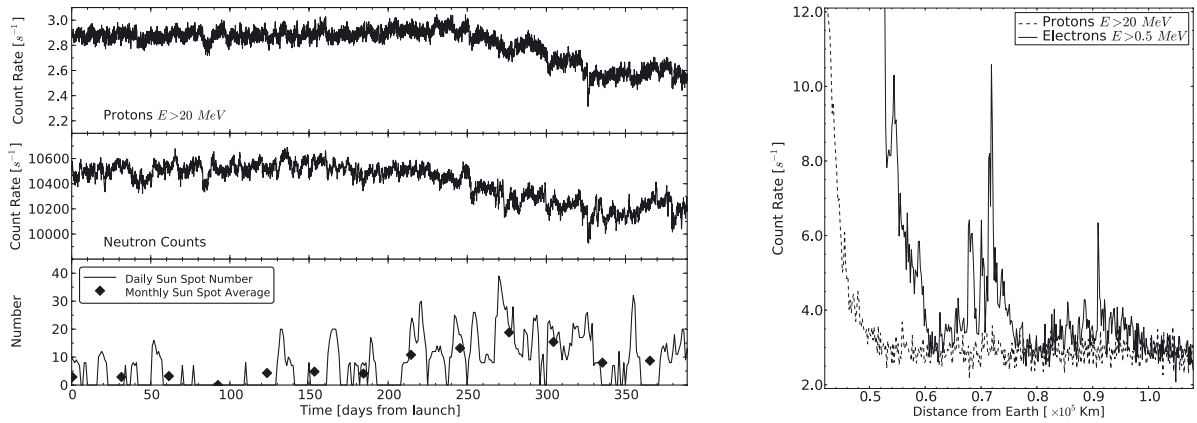

Fig. 8. *The top left panel* shows the time evolution of an SREM measure (TC1, Buehler et al. 1996) which is sensitive to high-energy protons. The levels shortly after launch are also indicated (on *the right*), showing the passage through the van Allen radiation belts, characterised by very high count levels. *The bottom panel* (on *the left*) shows the corresponding evolution of the sunspot number, indicating the slow transition of the solar cycle out of its current minimum. A monitor of high-energy neutrons (in this case located at McMurdo station, data courtesy of Bartol Research Institute, supported by US NSF), presented in *the middle panel*, traces the corresponding decrease in the flux of Galactic cosmic rays as the Sun becomes more active.

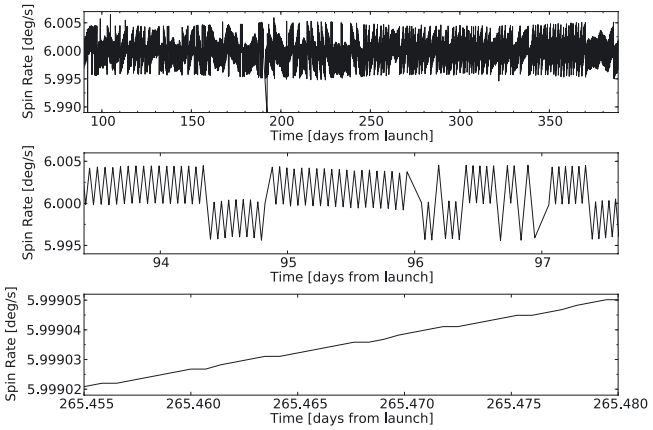

Fig. 9. *The top panel* shows the measured spin rate over the coverage period, which is always within ±0.1% of 1 rpm. The spin rate typically adopts one of three values as can be seen in *the middle panel*, which is a zoom into a period of several days. In *the bottom panel* we show the typical drift of the spin rate within a dwell, due to small residual torques applied to the satellite.

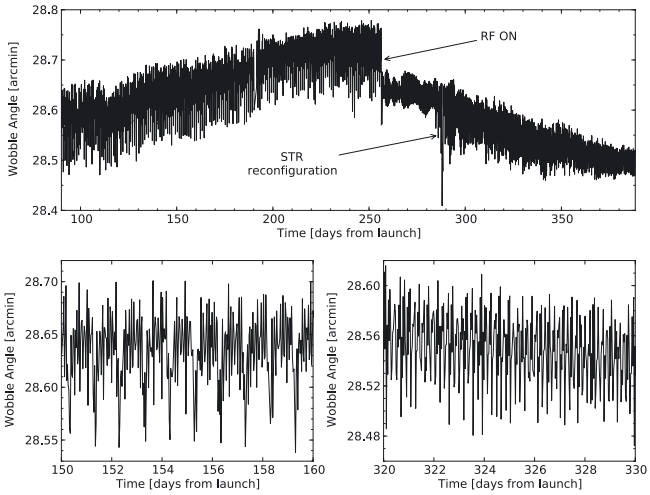

Fig. 10. *Top*: evolution of the measured offset between the principal axis of inertia and the geometric axis of the satellite (one point is plotted for each dwell period of approximately 50 min). The time variations observed are not real changes in the offset angle, but are instead due to thermoelastic deformations in the panel that supports the star trackers. *Bottom*: zooming in on short periods of time before (*left*) and after (*right*) the RF transponder was turned permanently on, reveals periodic variations (before, dominated by the daily RF On-Off switching; after, dominated by thermal control cycling of nearby units with typically one hour periodicity).

The principal axis of inertia, about which *Planck* rotates, is offset from the geometric axis by ∼28.6′ (see Fig. 10). The time evolution of the measured offset angle shows a long-timescale variation which is clearly linked to the seasonal power input variations on the solar array; this effect is not a real variation of the offset angle but is instead due to a thermoelastic deformation of the SVM panel that holds the star trackers[7]. Other thermoelastic deformations that give rise to similar effects are related to specific operations which have a thermal impact (see Fig. 10). The dominant (false) offset angle variation before 25 January 2010 is due to the daily thermal impact of the RF transponder being switched on and off, and after that date it is related to thermal control cycles in electronic units located near the star trackers; the peak-to-peak amplitude of the effect is of order 0.15′ before and 0.08′ after 25 January. These effects can be correlated to the temperature of the units responsible. They easily mask the real variation of the offset angle, which is due to gradual depletion of the fuel and helium tanks, and is of order 2.5″ per month[8]. This real variation of the wobble causes a corresponding change over time of the radius of the circle which each detector traces on the sky.

As described in Tauber et al. (2010a), *Planck*'s spin axis is displaced by 2′ approximately every 50 min. A typical sequence of manoeuvres and dwells is illustrated in Fig. 11. Each manoeuvre is carried out as a sequence of three thrusts spaced over three minutes (1st impulse – two minutes wait – 2nd impulse – one

[7] However, it appears as real in the filtered attitude.

[8] The variation is approximately 5′ per 50 kg of fuel expended. ∼170 g month^{-1} are expended in scanning manoeuvres and ∼50 g in each orbital maintenance manoeuvre, currently performed once every 8 weeks. Approximately 215 g month^{-1} of helium are vented to space by the HFI dilution cooler.

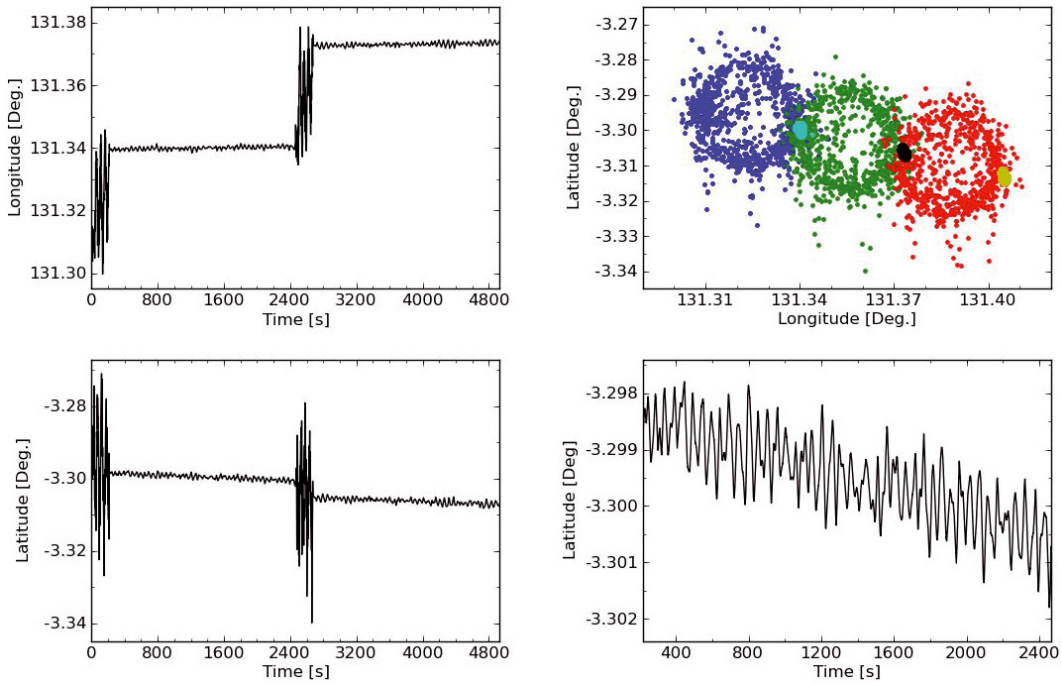

Fig. 11. *Left panels*: motion of the spin axis (i.e., the direction of the principal axis of inertia) in latitude (*top*) and longitude (*bottom*) as a function of time, over a typical period of 70 min, including two manoeuvres clearly identified by the large excursions in latitude and longitude. The dwell periods show the much smaller amplitude motions due to nutation and drift arising from solar radiation pressure. *Top right*: motion of the spin axis in Galactic latitude and longitude for a sequence of three manoeuvres and dwells. The attitude measurements during the slew are not filtered and are therefore very noisy; the measurements during each dwell are strongly clustered and show up as dense spots. *Bottom right*: zoom on a portion (about 30 min) of a dwell showing clearly the periodic motions which are a combination of the drift and residual nutation (period ∼5.4 min).

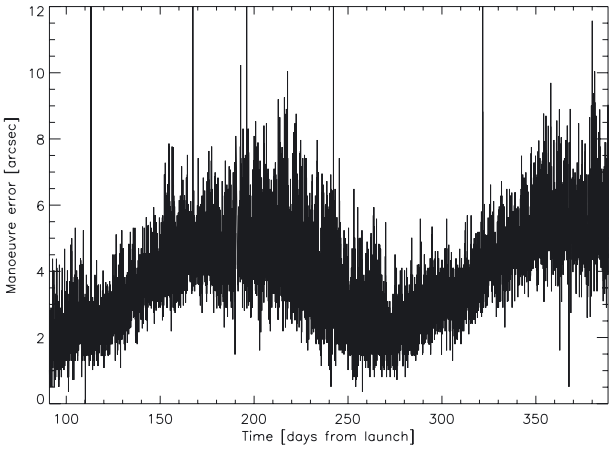

Fig. 12. The plot shows the difference between the achieved and commanded pointing after each 2′ manoeuvre; the difference is correlated with the duration of the previous dwell (see text). The vertical lines correspond to the very few occasions when the manoeuvre sequence did not execute as planned, resulting in anomalously high pointing errors.

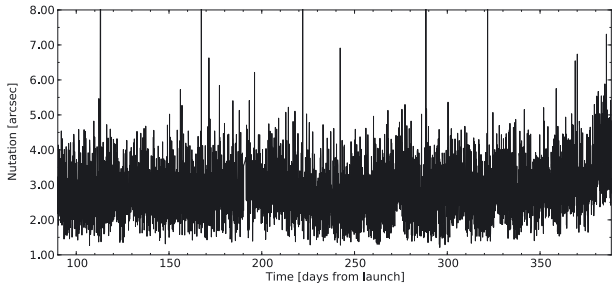

Fig. 13. The peak amplitude of the residual nutation averaged within each dwell time, over the coverage period.

minute wait – 3rd impulse), designed to cancel nutation as much as possible. Each manoeuvre lasts an average of about 220 s, as defined by on-board software mode transitions[9], which are used on the ground to trigger the end and start times of attitude filtering.

The pointing achieved after each reorientation is of course not exactly the commanded one; the difference, which varies between 2 and 8″ during the coverage period, is shown in Fig. 12. This variation is systematically related to the duration of the dwell preceding the manoeuvre, since the preceding pointing drifts due to solar radiation pressure, and the angular amplitude of the following manoeuvre changes correspondingly. The thrust sequence required for each manoeuvre is computed on-board based on the known mass properties of the satellite and known thruster response functions; the error made on each manoeuvre is mainly driven by the (imperfect) on-board knowledge of these properties, and therefore depends systematically on the amplitude of the manoeuvre. On very few occasions (visible in Fig. 12), the thruster sequence performance did not execute as planned, and resulted in a much larger manoeuvre error.

Although the thruster sequence is designed to damp nutation, it does not do so perfectly. The peak amplitude of the residual nutation is typically 3″ and does not vary significantly in time (see Fig. 13). The period of the nutation is 5.425 ± 0.010 min,

[9] The "start" of the manoeuvre mode is defined when the first thrust command is issued, triggering the actual thrust up to a half a minute later, and the "end" takes place immediately after the last thrust in the manoeuvre sequence.

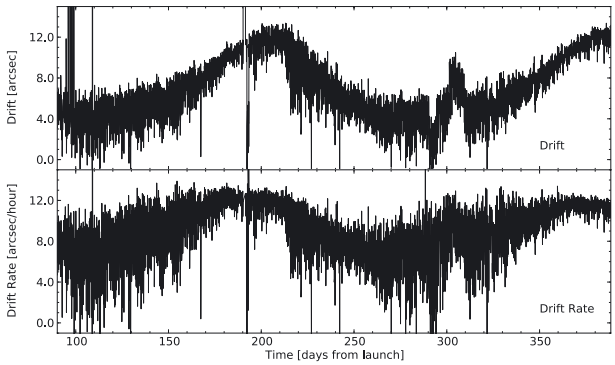

Fig. 14. The total drift due to solar radiation pressure within each dwell, which depends on the time length of the dwell (see Fig. 3). The drift rate (shown in *the lower panel*) is approximately constant at ∼9″ h^{-1}.

Table 2. *Planck* pointing performance.

	Median	Std. dev.	Unit
Spin rate	6.0001	0.0027	deg s^{-1}
Small manoeuvre accuracy	3.6	1.8	arcsec
Residual nutation amplitude after manoeuvre	2.68	1.75	arcsec
Drift rate during inertial pointing	9.14	3.0	arcsec h^{-1}

determined by the inertial properties of the satellite. Neither the amplitude nor the period of the nutation are observed to drift during a dwell period.

The last major characteristic of pointing within dwells is the drift due to solar radiation pressure. The total amplitude of the drift within each dwell varies between ∼5 and ∼12″, depending on the duration of each dwell (see Fig. 14). The rate of drift varies between ∼4 and ∼10″ h^{-1}, weakly correlated with the Solar Aspect Angle (which varies by very small amounts throughout the mission).

The pointing characteristics described above are summarised in Table 2.

5. Payload performance

The performance of the payload (i.e., two instruments and telescope) is described in detail in (Mennella et al. 2011, LFI) and (Planck HFI Core Team 2011a, HFI), and summarised in Table 3. We note that:

- the angular resolution measured on planets is within a few per cent of that predicted on the ground (Tauber et al. 2010b);
- the instantaneous sensitivity of the *Planck* LFI (Mennella et al. 2011) and HFI (Planck HFI Core Team 2011a) channels is estimated to be approximately 10% larger than that measured on the ground and extrapolated to launch conditions (Tauber et al. 2010a). For LFI the excess is understood to be due to inaccuracy in the calibration constants as measured in ground tests (Mennella et al. 2011); for HFI it is expected to be due to systematic effects remaining in the data at the current level of processing (Planck HFI Core Team 2011a);
- the photometric calibration uncertainty quoted is conservatively based on the current knowledge of systematic effects and data processing pipelines (Zacchei et al. 2011; Planck HFI Core Team 2011b). There is no reason to believe that the mission goals (1% in CMB channels and 3% at the highest frequencies) will not be reached for all *Planck* channels in due time;
- the point source sensitivities quoted correspond to the fluxes of the faintest sources included in the ERCSC (Planck Collaboration 2011c). Since the ERCSC is a high-reliability catalogue, based on very robust extraction from only the first all-sky survey, these levels will certainly improve substantially in the legacy catalogues which will be delivered in January 2013.

Table 3 confirms the findings of the early CPV activities, namely that the basic performance parameters of the scientific payload of *Planck* are very close to what was expected based on the measurements made on the ground before launch.

The ultimate performance of *Planck* also depends on its operational lifetime. *Planck* is a cryogenic mission (Planck Collaboration 2011b), whose nominal lifetime in routine operations (i.e., excluding transfer to orbit, commissioning and performance verification phases) was initially set to 15 months, allowing it to complete two full surveys of the sky within that period. Its actual lifetime is limited by the active coolers required to operate the *Planck* detectors, as listed hereafter.

- A ^{3}He-^{4}He dilution refrigerator, which cools the HFI bolometers to 0.1 K. The ^{3}He and ^{4}He gas are stored in tanks and vented to space after the dilution process. In-flight measurements of tank depletion predict that the ^{3}He gas will run out at the end of January 2012 (Planck Collaboration 2011b).
- A hydrogen sorption refrigerator, which cools the LFI radiometers to 20 K and provides a first pre-cooling stage for the HFI bolometer system. Its lifetime is limited by gradual degradation of the sorbent material. Two units fly on Planck: the first has provided cooling until August 2010; the second came into operation thereafter and is currently predicted to allow operation until December 2011 (Planck Collaboration 2011b). A further increase of lifetime may be obtained by applying on board the process of "regeneration" to the material.

Overall, the cooling system lifetime is at least one year above the nominal mission span, and no other spacecraft or payload factors impose additional limitations. Therefore, barring unexpected failures, *Planck* will continue surveying the sky until at least the end of 2011.

6. Conclusions

This paper summarises the performance of the *Planck* satellite during its first year of survey operations, in the areas most relevant for scientific analysis of the *Planck* data. Detailed descriptions of all aspects of the payload are provided in accompanying papers in this issue. It can be concluded that the major elements of the satellite's performance exceed their original technical requirements, and the scientific performance approaches the mission goals.

After an astoundingly smooth first year of survey operations, *Planck* continues to observe the sky and gather high quality scientific data, and is expected to do so as long as the cryogenic chain can keep the 100 mK stage near its nominal temperature, i.e., to the end of 2011 or possibly early 2012. Following the end of mission operations, the next major milestone in the project will be the release of the first set of timeline and map data products, currently foreseen in January 2013.

Table 3. *Planck* performance parameters determined from flight data.

channel	$N_{\rm detectors}$[a]	$\nu_{\rm center}$[b] [GHz]	mean beam[c] FWHM	mean beam[c] ellipticity	White-noise[d] sensitivity [$\mu K_{\rm RJ}\,{\rm s}^{1/2}$]	White-noise[d] sensitivity [$\mu K_{\rm CMB}\,{\rm s}^{1/2}$]	calibration[e] uncertainty [%]	faintest source[f] in ERCSC $\lvert b\rvert > 30°$ [mJy]
30 GHz	4	28.5	32.65	1.38	143.4	146.8	1	480
44 GHz	6	44.1	27.92	1.26	164.7	173.1	1	585
70 GHz	12	70.3	13.01	1.27	134.7	152.6	1	481
100 GHz	8	100	9.37	1.18	17.3	22.6	2	344
143 GHz	11	143	7.04	1.03	8.6	14.5	2	206
217 GHz	12	217	4.68	1.14	6.8	20.6	2	183
353 GHz	12	353	4.43	1.09	5.5	77.3	2	198
545 GHz	3	545	3.80	1.25	4.9	...	7	381
857 GHz	3	857	3.67	1.03	2.1	...	7	655

Notes. [(a)] For 30, 44, and 70 GHz, each "detector" is a linearly polarised radiometer. There are two (orthogonally polarized) radiometers behind each horn. Each radiometer has two diodes, both switched at high frequency between the sky and a blackbody load at ~4 K (Mennella et al. 2011). For 100 GHz and above, each "detector" is a bolometer (Planck HFI Core Team 2011a). Most of the bolometers are sensitive to polarisation, in which case there are two orthogonally polarised detectors behind each horn; some of the detectors are spider-web bolometers (one per horn) sensitive to the total incident power.
[(b)] Mean center frequency of the N detectors at each frequency.
[(c)] Mean optical properties of the N beams at each frequency; FWHM ≡ FWHM of circular Gaussian with the same volume. Ellipticity gives the ratio of major axis to minor axis for a best-fit elliptical Gaussian. In the case of HFI, the mean values quoted are the result of averaging the values of total-power and polarisation-sensitive bolometers, weighted by the number of channels and after removal of those affected by random telegraphic noise. The actual point spread function of an unresolved object on the sky depends not only on the optical properties of the beam, but also on sampling and time domain filtering in signal processing, and the way the sky is scanned. For details on these aspects see Sect. 4 of Mennella et al. (2011), Sect. 4 of Zacchei et al. (2011), Sect. 4.2 of Planck HFI Core Team (2011a), and Sect. 6.2 of Planck HFI Core Team (2011b).
[(d)] Uncorrelated noise on the sky in 1 s for the array of N detectors, in Rayleigh-Jeans units and in thermodynamic CMB units. For a preliminary discussion of correlated noise and systematic effects, see Mennella et al. (2011), Planck HFI Core Team (2011a), Zacchei et al. (2011), and Planck HFI Core Team (2011b).
[(e)] Absolute uncertainty, based on the known amplitude of the CMB dipole up to 353 GHz, and on FIRAS at 545 and 857 GHz (Zacchei et al. 2011; Planck HFI Core Team 2011b).
[(f)] Flux density of the faintest source included in the ERCSC (Planck Collaboration 2011c).

Acknowledgements. *Planck* is too large a project to allow full acknowledgement of all contributions by individuals, institutions, industries, and funding agencies. The main entities involved in the mission operations are as follows. The European Space Agency operates the satellite via its Mission Operations Centre located at ESOC (Darmstadt, Germany) and coordinates scientific operations via the *Planck* Science Office located at ESAC (Madrid, Spain). Two Consortia, comprising around 100 scientific institutes within Europe, the USA, and Canada, and funded by agencies from the participating countries, developed the scientific instruments LFI and HFI, and continue to operate them via Instrument Operations Teams located in Trieste (Italy) and Orsay (France). The Consortia are also responsible for scientific processing of the acquired data. The Consortia are led by the Principal Investigators: J.-L. Puget in France for HFI (funded principally by CNES and CNRS/INSU-IN2P3) and N. Mandolesi in Italy for LFI (funded principally via ASI). NASA's US *Planck* Project, based at JPL and involving scientists at many US institutions, contributes significantly to the efforts of these two Consortia. A third Consortium, led by H. U. Norgaard-Nielsen and supported by the Danish Natural Research Council, contributed to the reflector programme. The author list for this paper has been selected by the *Planck* Science Team from the Planck Collaboration, and is composed of individuals from all of the above entities who have made multi-year contributions to the development of the mission. It does not pretend to be inclusive of all contributions. A description of the Planck Collaboration and a list of its members, indicating which technical or scientific activities they have been involved in, can be found at (http://www.rssd.esa.int/index.php?project=PLANCK\&page=Planck_Collaboration). The Planck Collaboration acknowledges the support of: ESA; CNES and CNRS/INSU-IN2P3-INP (France); ASI, CNR, and INAF (Italy); NASA and DoE (USA); STFC and UKSA (UK); CSIC, MICINN and JA (Spain); Tekes, AoF and CSC (Finland); DLR and MPG (Germany); CSA (Canada); DTU Space (Denmark); SER/SSO (Switzerland); RCN (Norway); SFI (Ireland); FCT/MCTES (Portugal); and DEISA (EU).

References

Bersanelli, M., Mandolesi, N., Butler, R. C., et al. 2010, A&A, 520, A4
Buehler, P., Desorgher, L., & Zehnder, A. 1996, in Environment Modeling for Space-Based Applications, ed. T.-D. Guyenne, & A. Hilgers, ESA SP, 392, 87
Górski, K. M., Hivon, E., Banday, A. J., et al. 2005, ApJ, 622, 759
Lamarre, J., Puget, J., Ade, P. A. R., et al. 2010, A&A, 520, A9
Mennella, A., Bersanelli, M., Butler, R. C., et al. 2011, A&A, 536, A3
Planck Collaboration 2005, ESA publication ESA-SCI(2005)/01
Planck Collaboration 2011a, A&A, 536, A1
Planck Collaboration 2011b, A&A, 536, A2
Planck Collaboration 2011c, A&A, 536, A7
Planck Collaboration 2011d, A&A, 536, A8
Planck Collaboration 2011e, A&A, 536, A9
Planck Collaboration 2011f, A&A, 536, A10
Planck Collaboration 2011g, A&A, 536, A11
Planck Collaboration 2011h, A&A, 536, A12
Planck Collaboration 2011i, A&A, 536, A13
Planck Collaboration 2011j, A&A, 536, A14
Planck Collaboration 2011k, A&A, 536, A15
Planck Collaboration 2011l, A&A, 536, A16
Planck Collaboration 2011m, A&A, 536, A17
Planck Collaboration 2011n, A&A, 536, A18
Planck Collaboration 2011o, A&A, 536, A19
Planck Collaboration 2011p, A&A, 536, A20
Planck Collaboration 2011q, A&A, 536, A21
Planck Collaboration 2011r, A&A, 536, A22
Planck Collaboration 2011s, A&A, 536, A23
Planck Collaboration 2011t, A&A, 536, A24
Planck Collaboration 2011u, A&A, 536, A25
Planck Collaboration 2011v, The Explanatory Supplement to the Planck Early Release Compact Source Catalogue (ESA)
Planck Collaboration 2011w, A&A, 536, A26
Planck HFI Core Team 2011a, A&A, 536, A4
Planck HFI Core Team 2011b, A&A, 536, A6
Tauber, J. A., Mandolesi, N., Puget, J., et al. 2010a, A&A, 520, A1
Tauber, J. A., Norgaard-Nielsen, H. U., Ade, P. A. R., et al. 2010b, A&A, 520, A2
Zacchei, A., Maino, D., Baccigalupi, C., et al. 2011, A&A, 536, A5

[1] Aalto University Metsähovi Radio Observatory, Metsähovintie 114, 02540 Kylmälä, Finland
[2] Agenzia Spaziale Italiana Science Data Center, c/o ESRIN, via Galileo Galilei, Frascati, Italy
[3] Astroparticule et Cosmologie, CNRS (UMR7164), Université Denis Diderot Paris 7, Bâtiment Condorcet, 10 rue A. Domon et Léonie Duquet, Paris, France
[4] Astrophysics Group, Cavendish Laboratory, University of Cambridge, J J Thomson Avenue, Cambridge CB3 0HE, UK
[5] Atacama Large Millimeter/submillimeter Array, ALMA Santiago Central Offices, Alonso de Cordova 3107, Vitacura, Casilla 763 0355, Santiago, Chile
[6] CITA, University of Toronto, 60 St. George St., Toronto, ON M5S 3H8, Canada
[7] CNES, 18 avenue Edouard Belin, 31401 Toulouse Cedex 9, France
[8] CNR – ISTI, Area della Ricerca, via G. Moruzzi 1, Pisa, Italy
[9] CNRS, IRAP, 9 Av. colonel Roche, BP 44346, 31028 Toulouse Cedex 4, France
[10] California Institute of Technology, Pasadena, California, USA
[11] Centre of Mathematics for Applications, University of Oslo, Blindern, Oslo, Norway
[12] DAMTP, University of Cambridge, Centre for Mathematical Sciences, Wilberforce Road, Cambridge CB3 0WA, UK
[13] DSM/Irfu/SPP, CEA-Saclay, 91191 Gif-sur-Yvette Cedex, France
[14] DTU Space, National Space Institute, Juliane Mariesvej 30, Copenhagen, Denmark
[15] Departamento de Física, Universidad de Oviedo, Avda. Calvo Sotelo s/n, Oviedo, Spain
[16] Department of Astronomy and Astrophysics, University of Toronto, 50 Saint George Street, Toronto, Ontario, Canada
[17] Department of Physics & Astronomy, University of British Columbia, 6224 Agricultural Road, Vancouver, British Columbia, Canada
[18] Department of Physics and Astronomy, University of Southern California, Los Angeles, California, USA
[19] Department of Physics, Gustaf Hällströmin katu 2a, University of Helsinki, Helsinki, Finland
[20] Department of Physics, Princeton University, Princeton, New Jersey, USA
[21] Department of Physics, Purdue University, 525 Northwestern Avenue, West Lafayette, Indiana, USA
[22] Department of Physics, University of California, Berkeley, California, USA
[23] Department of Physics, University of California, One Shields Avenue, Davis, California, USA
[24] Department of Physics, University of California, Santa Barbara, California, USA
[25] Department of Physics, University of Illinois at Urbana-Champaign, 1110 West Green Street, Urbana, Illinois, USA
[26] Dipartimento di Fisica G. Galilei, Università degli Studi di Padova, via Marzolo 8, 35131 Padova, Italy
[27] Dipartimento di Fisica, Università La Sapienza, P. le A. Moro 2, Roma, Italy
[28] Dipartimento di Fisica, Università degli Studi di Milano, via Celoria 16, Milano, Italy
[29] Dipartimento di Fisica, Università degli Studi di Trieste, via A. Valerio 2, Trieste, Italy
[30] Dipartimento di Fisica, Università di Ferrara, via Saragat 1, 44122 Ferrara, Italy
[31] Dipartimento di Fisica, Università di Roma Tor Vergata, via della Ricerca Scientifica 1, Roma, Italy
[32] Discovery Center, Niels Bohr Institute, Blegdamsvej 17, Copenhagen, Denmark
[33] Dpto. Astrofísica, Universidad de La Laguna (ULL), 38206 La Laguna, Tenerife, Spain
[34] European Southern Observatory, ESO Vitacura, Alonso de Cordova 3107, Vitacura, Casilla 19001, Santiago, Chile
[35] European Space Agency, ESAC, Camino bajo del Castillo, s/n, Urbanización Villafranca del Castillo, Villanueva de la Cañada, Madrid, Spain
[36] European Space Agency, ESAC, Planck Science Office, Camino bajo del Castillo, s/n, Urbanización Villafranca del Castillo, Villanueva de la Cañada, Madrid, Spain
[37] European Space Agency, ESOC, Robert-Bosch-Str. 5, Darmstadt, Germany
[38] European Space Agency, ESTEC, Keplerlaan 1, 2201 AZ Noordwijk, The Netherlands
[39] Haverford College Astronomy Department, 370 Lancaster Avenue, Haverford, Pennsylvania, USA
[40] Helsinki Institute of Physics, Gustaf Hällströmin katu 2, University of Helsinki, Helsinki, Finland
[41] INAF – Osservatorio Astrofisico di Catania, via S. Sofia 78, Catania, Italy
[42] INAF – Osservatorio Astronomico di Padova, Vicolo dell'Osservatorio 5, Padova, Italy
[43] INAF – Osservatorio Astronomico di Roma, via di Frascati 33, Monte Porzio Catone, Italy
[44] INAF – Osservatorio Astronomico di Trieste, via G.B. Tiepolo 11, Trieste, Italy
[45] INAF/IASF Bologna, via Gobetti 101, Bologna, Italy
[46] INAF/IASF Milano, via E. Bassini 15, Milano, Italy
[47] INRIA, Laboratoire de Recherche en Informatique, Université Paris-Sud 11, Bâtiment 490, 91405 Orsay Cedex, France
[48] INSU, Institut des sciences de l'univers, CNRS, 3 rue Michel-Ange, 75794 Paris Cedex 16, France
[49] IPAG: Institut de Planétologie et d'Astrophysique de Grenoble, Université Joseph Fourier, Grenoble 1/CNRS-INSU, UMR 5274, 38041 Grenoble, France
[50] ISDC Data Centre for Astrophysics, University of Geneva, ch. d'Ecogia 16, Versoix, Switzerland
[51] Imperial College London, Astrophysics group, Blackett Laboratory, Prince Consort Road, London, SW7 2AZ, UK
[52] Infrared Processing and Analysis Center, California Institute of Technology, Pasadena, CA 91125, USA
[53] Institut Néel, CNRS, Université Joseph Fourier Grenoble I, 25 rue des Martyrs, Grenoble, France
[54] Institut d'Astrophysique Spatiale, CNRS (UMR8617) Université Paris-Sud 11, Bâtiment 121, Orsay, France
[55] Institut d'Astrophysique de Paris, CNRS UMR7095, Université Pierre & Marie Curie, 98 bis boulevard Arago, Paris, France
[56] Institut de Ciències de l'Espai, CSIC/IEEC, Facultat de Ciències, Campus UAB, Torre C5 par-2, Bellaterra 08193, Spain
[57] Institute for Space Sciences, Bucharest-Magurale, Romania
[58] Institute of Astronomy and Astrophysics, Academia Sinica, Taipei, Taiwan
[59] Institute of Astronomy, University of Cambridge, Madingley Road, Cambridge CB3 0HA, UK
[60] Institute of Theoretical Astrophysics, University of Oslo, Blindern, Oslo, Norway
[61] Instituto de Astrofísica de Canarias, C/Vía Láctea s/n, La Laguna, Tenerife, Spain
[62] Instituto de Física de Cantabria (CSIC-Universidad de Cantabria), Avda. de los Castros s/n, Santander, Spain
[63] Istituto di Fisica del Plasma, CNR-ENEA-EURATOM Association, via R. Cozzi 53, Milano, Italy
[64] Jet Propulsion Laboratory, California Institute of Technology, 4800 Oak Grove Drive, Pasadena, California, USA
[65] Jodrell Bank Centre for Astrophysics, Alan Turing Building, School of Physics and Astronomy, The University of Manchester, Oxford Road, Manchester, M13 9PL, UK
[66] Kavli Institute for Cosmology Cambridge, Madingley Road, Cambridge, CB3 0HA, UK
[67] LERMA, CNRS, Observatoire de Paris, 61 avenue de l'Observatoire, Paris, France
[68] Laboratoire AIM, IRFU/Service d'Astrophysique - CEA/DSM - CNRS - Université Paris Diderot, Bât. 709, CEA-Saclay, 91191 Gif-sur-Yvette Cedex, France
[69] Laboratoire Traitement et Communication de l'Information, CNRS (UMR 5141) and Télécom ParisTech, 46 rue Barrault, 75634 Paris Cedex 13, France

[70] Laboratoire de Physique Subatomique et de Cosmologie, CNRS/IN2P3, Université Joseph Fourier Grenoble I, Institut National Polytechnique de Grenoble, 53 rue des Martyrs, 38026 Grenoble Cedex, France
[71] Laboratoire de l'Accélérateur Linéaire, Université Paris-Sud 11, CNRS/IN2P3, Orsay, France
[72] Lawrence Berkeley National Laboratory, Berkeley, California, USA
[73] Max-Planck-Institut für Astrophysik, Karl-Schwarzschild-Str. 1, 85741 Garching, Germany
[74] MilliLab, VTT Technical Research Centre of Finland, Tietotie 3, Espoo, Finland
[75] National University of Ireland, Department of Experimental Physics, Maynooth, Co. Kildare, Ireland
[76] Niels Bohr Institute, Blegdamsvej 17, Copenhagen, Denmark
[77] Observational Cosmology, Mail Stop 367-17, California Institute of Technology, Pasadena, CA, 91125, USA
[78] Optical Science Laboratory, University College London, Gower Street, London, UK
[79] Rutherford Appleton Laboratory, Chilton, Didcot, UK
[80] SISSA, Astrophysics Sector, via Bonomea 265, 34136, Trieste, Italy
[81] SUPA, Institute for Astronomy, University of Edinburgh, Royal Observatory, Blackford Hill, Edinburgh EH9 3HJ, UK
[82] School of Physics and Astronomy, Cardiff University, Queens Buildings, The Parade, Cardiff, CF24 3AA, UK
[83] Space Research Institute (IKI), Russian Academy of Sciences, Profsoyuznaya Str 84/32, Moscow 117997, Russia
[84] Space Sciences Laboratory, University of California, Berkeley, California, USA
[85] Spitzer Science Center, 1200 E. California Blvd., Pasadena, California, USA
[86] Stanford University, Dept of Physics, Varian Physics Bldg, 382 via Pueblo Mall, Stanford, California, USA
[87] Thales Alenia Space France, 100 Boulevard du Midi, Cannes la Bocca, France
[88] Universität Heidelberg, Institut für Theoretische Astrophysik, Albert-Überle-Str. 2, 69120 Heidelberg, Germany
[89] Université de Toulouse, UPS-OMP, IRAP, 31028 Toulouse Cedex 4, France
[90] Universities Space Research Association, Stratospheric Observatory for Infrared Astronomy, MS 211-3, Moffett Field, CA 94035, USA
[91] University of Granada, Departamento de Física Teórica y del Cosmos, Facultad de Ciencias, Granada, Spain
[92] University of Miami, Knight Physics Building, 1320 Campo Sano Dr., Coral Gables, Florida, USA
[93] Warsaw University Observatory, Aleje Ujazdowskie 4, 00-478 Warszawa, Poland